Sensors & Transducers, Vol. 270, Issue 3, November 2025, pp. 30-39

www.sensorsportal.com

Sensors & Transducers

Published by IFSA Publishing, S. L., 2025
http://www.sensorsportal.com

Machine-learning-based Evaluation of Upper Limb Motion Using 8×8 Time-of-flight and LiDAR Sensors: SVM Classification and Deep Neural Network Analysis

[1, *] Yasutaka UCHIDA, [1] Eiichi OHKUBO, [1] Manami NISHI, [2] Tomoko FUNAYAMA and [3] Yoshiaki KOGURE

[1] Teikyo University of Science, Dept. of Life Science, Adachi-ku, 120-0045 Tokyo, Japan
[2] Teikyo University of Science, Dept. of Occupational therapy, Uenohara-shi, 409-0193 Yamanashi, Japan
[3] Teikyo University of Science, professor emeritus, Adachi-ku, 120-0045 Tokyo, Japan
[1] Tel.: +81369101010, Fax: +81369103800
E-mail: uchida@ntu.ac.jp

Received: 30 May 2025 / Revised:10 Nov. 2025 / Accepted:18 Nov. 2025 / Published: 28 Nov. 2025

Abstract: Upper limb rehabilitation methods, such as the table sliding technique and pegboard exercises, are widely used because of their low physical burden on patients. A critical aspect of these methods is the ability to evaluate whether the exercises are appropriate for the patient's condition and objectively assess the recovery progress. Traditionally, therapists have relied on direct observations and predefined evaluation criteria to assess movement performance and recovery. However, these approaches often require specialized equipment and technical expertise. To address these limitations, inertial measurement units (IMUs) have been proposed as a means of quantifying task performance and supporting clinical decision-making using objective data. Our previous studies, presented at SEIA'2024 and published in *Sensors and Transducers*, explored the application of IMUs in upper limb rehabilitation. However, challenges remain regarding sensor miniaturization and simultaneous multisensor measurements, owing to peg-size constraints. Recent advancements in time-of-flight (ToF) sensor technology have enabled the development of compact and cost-effective sensors. ToF sensors offer privacy advantages by not capturing direct images, making them suitable for healthcare applications. In this study, we compared two types of ToF-based sensors: one that detects object presence within an 8×8 pixel area based on height and another that uses 360° infrared light to measure object positions in 2D. We first applied support vector machine classification to the images obtained from both sensors, followed by classification using TensorFlow. The results were analyzed to evaluate the differences in the classification accuracy between the two sensor types and methods.

Keywords: Time of flight, LiDAR, Raspberry Pi, Upper limb rehabilitation, SVM, TensorFlow.

1. Introduction

Representative methods for upper limb rehabilitation include the table sliding and pegboard methods, both of which are widely used because of their ability to avoid excessive strain on the upper limbs [1-7]. A key aspect of these methods is the ability to evaluate whether the exercises and treatments are appropriate for the patient's condition and level and to objectively assess the degree of recovery. These approaches are effective tools for supporting medical rehabilitation and healthcare.

Typically, physical and occupational therapists directly observe upper limb movements, such as peg transfers and movement speed, and assess recovery based on predefined evaluation criteria related to treatment duration and movement performance [8-13]. To objectively quantify upper limb movements, motion capture systems using markers are commonly employed, and methods for measuring touch actions on computer screens have been proposed. However, these approaches require dedicated equipment and proficiency in operating the devices, which presents certain challenges.

To address these issues, methods that use inertial measurement units (IMUs) attached to the subject have been proposed to evaluate task performance levels, thereby enabling the acquisition of numerical data to support therapists' empirical judgments. We previously reported the results of basic system evaluations for applying IMUs to upper limb rehabilitation in SEIA' 2024 [14, 15] and the journal *Sensors and Transducers* [16]. However, limitations in peg size have made it difficult to miniaturize IMU sensors, and challenges remain in simultaneous measurements using multiple IMUs.

Recently, rapid advancements in time-of-flight (ToF) sensor technology have led to the miniaturization and cost reduction of sensors. ToF methods offer privacy advantages by not capturing direct images of the subjects, making them suitable for a wide range of applications [16].

In this study, we compared two types of ToF-based sensors: one that detects the presence of objects within an 8×8 pixel area based on height detection and another that emits infrared light at 360° and measures object positions in 2D based on reflected light. To compare the classification accuracy, we first applied the support vector machine (SVM) method [17-20] to images obtained from the 8×8 ToF sensor and LiDAR. Next, we used TensorFlow [21-24] to perform the classification and examined the differences in the classification results between the two sensor types. Based on these results, we discuss the differences in the classification accuracy of each method.

2. Experiment

2.1. System Setup

Two measurement systems were used in this study. The first system combined an STMicroelectronics VL53L5CX ToF sensor with a Nucleo-F401RE evaluation board [25] (Fig. 1(a)). Although the evaluation board was relatively large (10 cm×15 cm), the sensor module was compact, measuring only 1.5 cm×3.0 cm (Fig. 1(b)). The sensor employed a vertical cavity surface-emitting laser with a diffractive optical element on top, projecting a square field of view (FoV) onto the scene. It measured absolute distances of up to 4.0 m regardless of the color or reflectivity of the target and could be operated at up to 60 Hz. The multizone ranges supported a grid of up to 8×8 pixels with a wide diagonal FoV of 63°.

The 8×8 ToF measurement system used the dedicated VL53L5CX GUI software from the manufacturer, which divided the PC display into 8×8 sections, the median distance for each zone was calculated, and the results are presented as a color-coded heatmap (Fig. 2). This identified 8×8 zones corresponding to the arm holding the peg. In the measurement setup (Fig. 3), both the sensor and webcam for position verification were placed in a simple cardboard housing, with the sensor mounted 53 cm above the measurement plane and covering an observation area of approximately 34 cm×34 cm. Although the manufacturer's software allows the camera image to be overlaid onto an 8×8 display, this function was not used in the experiment.

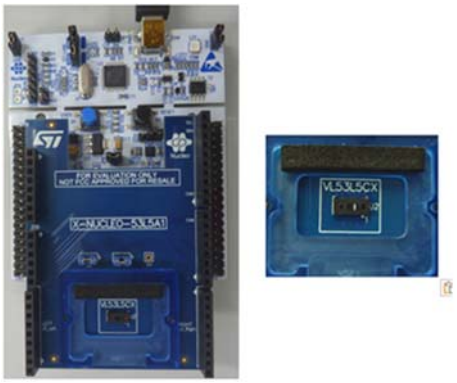

(a) Evaluation board; (b) ToF sensor.

Fig. 1. VL53L5CX ToF sensor with a Nucleo-F401RE evaluation board.

Fig. 2. Screen display of the VL53L5CX GUI software.

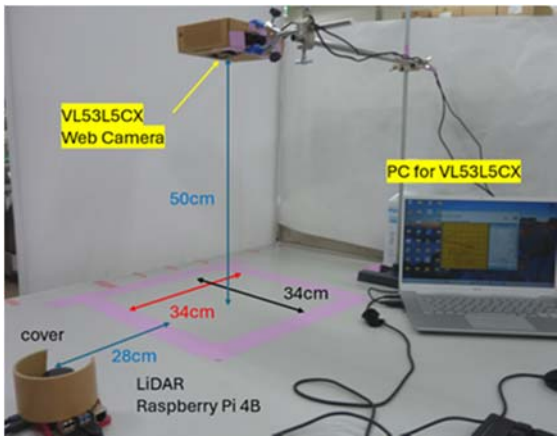

Fig. 3. Measurement setup.

The second system comprised an OKDO LD006 LiDAR unit [26] paired with a Raspberry Pi 4 B unit. The LiDAR used infrared light to perform 2D distance measurements within a range of 0.02–12 m over 360°,

with a rotation frequency of 10 Hz. The LiDAR unit was compact and fit a Raspberry Pi case, and Bluetooth connectivity facilitated its deployment in rehabilitation settings. For upper limb measurements, the cylindrical cover was partially removed to limit the measurement range to the tabletop area.

2.2. Classification Method of SVM

For the classification, three distinct arm positions that were considered relatively easy to distinguish were selected: (1) the arm extended toward the left front, (2) the arm extended toward the right front, and (3) the arm extended toward the left rear. For each position, 100 images in PNG format were used as training data, and 10 images were used as test data.

In the SVM approach, the image data were loaded using the imread function in OpenCV. From each image, the average values of the R, G, and B channels were extracted as a three-dimensional feature vector. This feature represents the overall color tendency of the image and was chosen for its simplicity and interpretability. The SVM model was designed to be classified based on color characteristics. The feature vectors were standardized to have a mean of zero and a variance of one. A linear kernel was used for the classification. The confusion matrix was visualized using a heatmap generated using the Seaborn Library. In addition, classification performance metrics, including precision, recall, and F1-score, were calculated to evaluate the model.

2.3. TensorFlow Classification Setting

In addition to SVM-based classification, a deep learning approach using TensorFlow was implemented to evaluate the classification performance. The model was constructed using a sequential architecture consisting of convolutional, pooled, and fully connected layers. The input images were resized to a fixed resolution and normalized to ensure consistent data preprocessing.

The training and test datasets consisted of 100 and 10 images per class, respectively. The model was trained using the Adam optimizer with a learning rate of 0.001. Categorical cross-entropy was used as the loss function, and training was conducted over 50 epochs with a batch size of 16. Early stopping was applied to prevent overfitting based on the validation loss monitoring.

To evaluate the classification performance, the accuracy. The model was implemented and trained using TensorFlow 2.20.0 and Keras APIs.

3. Results

3.1. Measurements Using the 8×8 ToF System

Fig. 4 shows a heatmap of the arm positions within an 8×8 zone. A heatmap was generated using a custom program developed for this study, which was separated from the display provided by the measurement software. The color variations correspond to the hand movements shown in the lower panel. During the measurements, the IMU sensor was intentionally held higher than the peg substitute to facilitate future trajectory analysis using IMU data. The heatmap captured distinct color changes corresponding to the left–right movements.

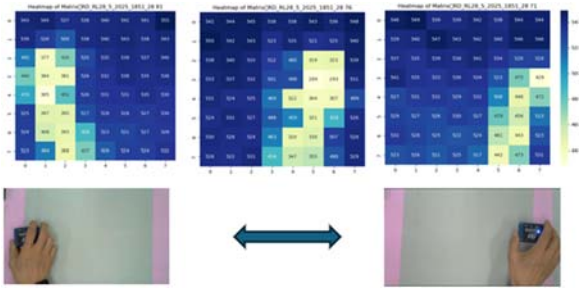

Fig. 4. Heatmap of arm positions within an 8×8 zone.

3.2. Verification of the 8×8 ToF Sensor Position Accuracy

The positional information obtained from the sensor was compared with the positions derived from video footage and those estimated from heatmap images. The verification was conducted for five reference positions relative to the participant: left forward, right forward, center, left near, and right near, as indicated in Fig. 5. The coordinates were calculated using proportional scaling, with the frame and tape widths set to 34 and 5 cm, respectively.

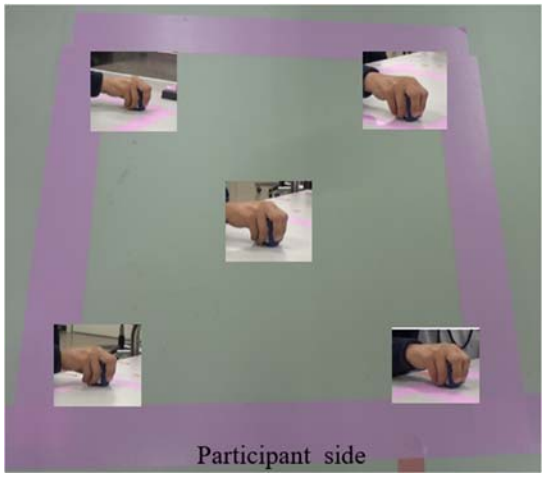

Fig. 5. Description of locations for assessing the accuracy of the measurement location.

Fig. 6 shows a heatmap based on the calculated results, whereas Fig. 7 shows a magnified view of the back of the left hand holding the peg substitute when the arm is extended left forward. For measurements in

the peripheral regions, the accuracy was almost same when the width of the back of the hand was considered. However, as shown in Fig. 7, the fingertip position shifted forward by approximately 1.8 cm. Similarly, a displacement of approximately 2.0 cm was observed when the arm was extended forward to the right. At the center position, the forward–backward displacement ranged from 1.1 cm to 1.6 cm, whereas the left–right displacement was approximately 3.6 cm to the left. When the arm was not extended toward the side of the participant, the measurement errors were approximately zero.

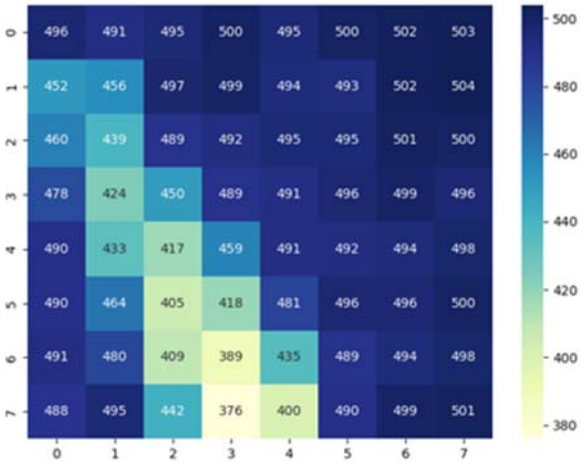

Fig. 6. Heatmap display based on the calculated results.

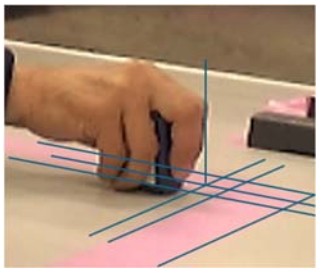

Fig. 7. Magnified view of the back of the left hand holding the peg.

3.3. Measurements Using LiDAR

Fig. 8 shows an example of the measurements taken when the participants placed their arms in a right-near position. These were displayed on Raspberry Pi. As the LiDAR measurements were performed at 360° and 10 Hz, the obtained comma-separated value (CSV) data size occasionally exceeded 0.4 MB/s. To address this problem, a portion of the cylindrical cover was removed to limit the measurement range and reduce the dataset to approximately 70 kB/s while retaining the target information. On the display, the participant is located at the top, whereas the LiDAR is indicated by a purple arc at the lower center. The blue points on the far left represent the wall of the measurement stand, and the adjacent purple cluster corresponds to the base of the support column holding the 8×8 ToF device.

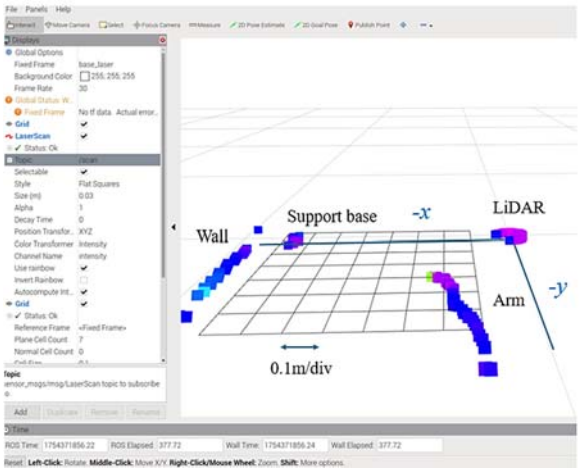

Fig. 8. Example of a LiDAR measurement display screen.

Fig. 9 shows an example in which the display is vertically transformed to align with a heatmap. The x- and y-axes are displayed as negative values, with the LiDAR positioned at the origin. Filter processing was used to restrict the data to a depth of 10–75 cm. In Fig. 9, this view is further magnified to match the corresponding heatmap regions. The blue, red, and green boxes represent the CSV data obtained from LiDAR, the area corresponding to the heatmap, and the area presumed to represent the back of the hand, respectively.

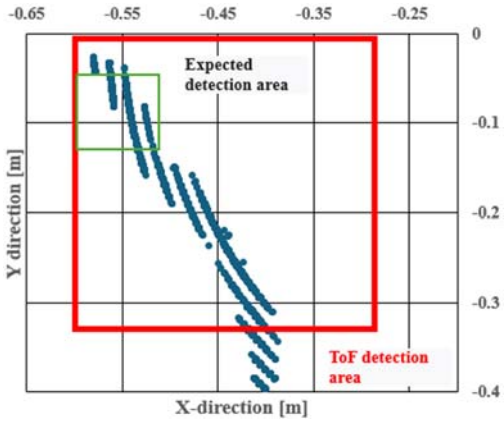

Fig. 9. Arm position calculated from the CSV data associated with the 8×8 ToF.

Fig. 10 shows a heatmap when the right arm was moved to the central area of the right edge of the 8×8 ToF measurement zone, and Fig. 11 shows the corresponding LiDAR data. In the heatmap, the area corresponding to the right arm spans six rows × two columns, whereas in the LiDAR display, points appear outside the red box because of the detection of the lateral surface of the arm.

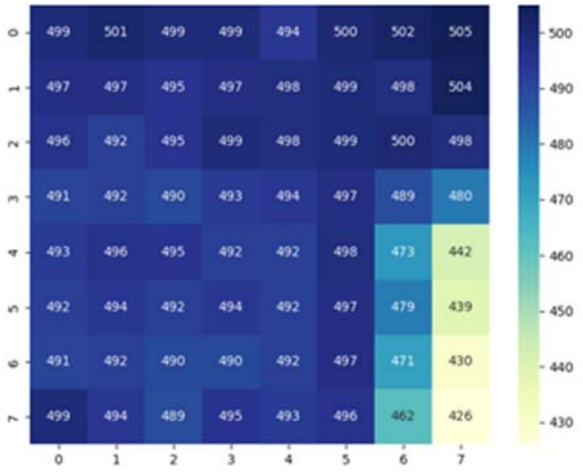

Fig. 10. Heatmap when the right arm was moved to the central area of the right edge of the 8×8 ToF measurement zone.

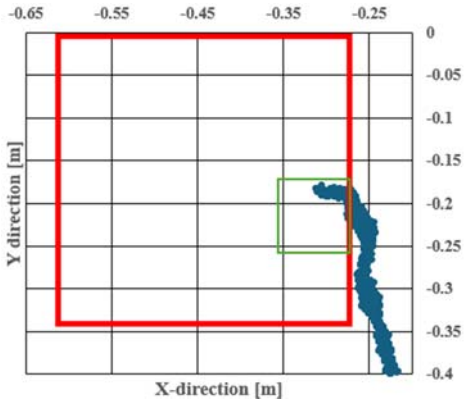

Fig. 11. Arm position calculated from the CSV data associated with the 8×8 ToF.

3.4. SVM Classification using 8×8 ToF System

Initially, classification was performed using heatmap visualizations with scale bars to assess model performance. Fig. 12 shows a 3D plot of the training data (a) and test data (b) classified using the SVM method.

The classification task involved three distinct arm positions: (1) left forward extension, (2) right forward extension, and (3) left backward extension. The back left corresponds to the hand position at the bottom left of Fig. 5. Each class was represented by the training and test datasets, with Class 0 corresponding to left-forward, Class 1 to right-forward, and Class 2 to left-backward. The confusion matrix is shown in Fig. 13, and the classification reports, including precision, recall, and F1-score, are listed in Table 1. The accuracy and model loss over epochs are illustrated in Figs. 14 and 15, respectively. These results indicated that the three movement patterns were classified with high accuracy.

To further evaluate the robustness of the classification program, an intentional modification was introduced: in the test dataset for the left-forward class, 5 out of 10 images were replaced with images from the right-forward class. The classification results for these conditions are shown in Fig. 16. The corresponding confusion matrix is shown in Fig. 17.

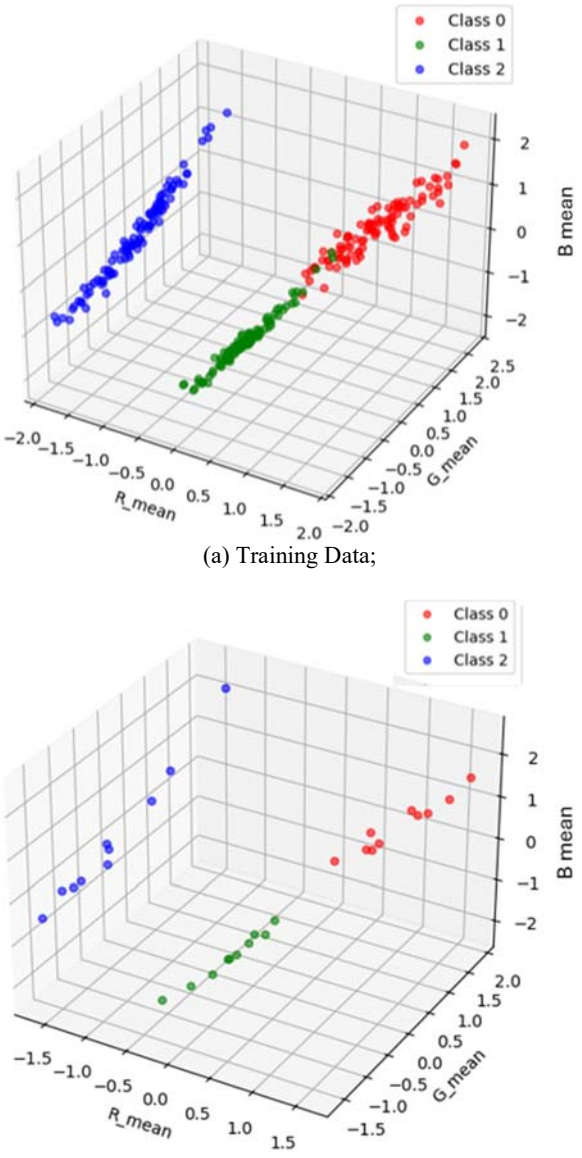

(a) Training Data;

(b) Test data.

Fig. 12. 3D plot of the training data (a) and test data (b) classified using the SVM method.

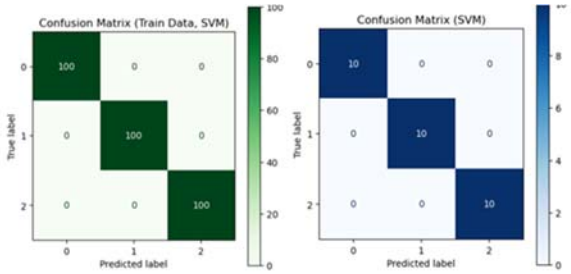

(a) Training data (b) Test data

Fig. 13. Confusion matrix.

Table 1. Classification report.

	precision	recall	f1-score	support
Class 0	1.0000	1.0000	1.0000	10
Class 1	1.0000	1.0000	1.0000	10
Class 2	1.0000	1.0000	1.0000	10
accuracy			1.0000	30
macro avg	1.0000	1.0000	1.0000	30
weighted avg	1.0000	1.0000	1.0000	30

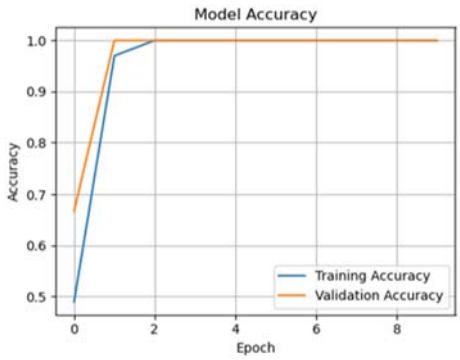

Fig. 14. Model accuracy.

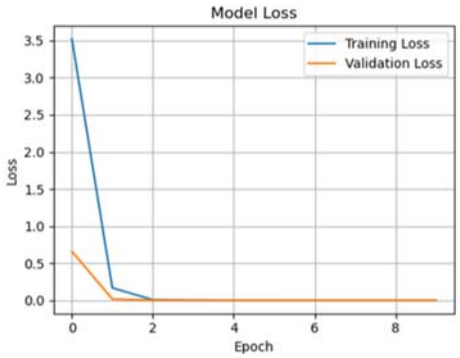

Fig. 15. Model loss.

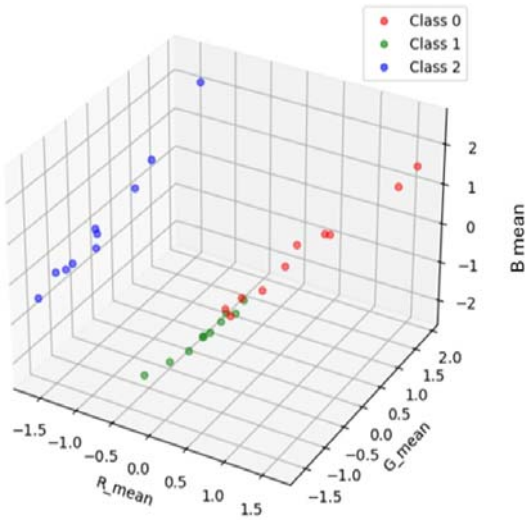

Fig. 16. 3D classification results of intentional modification.

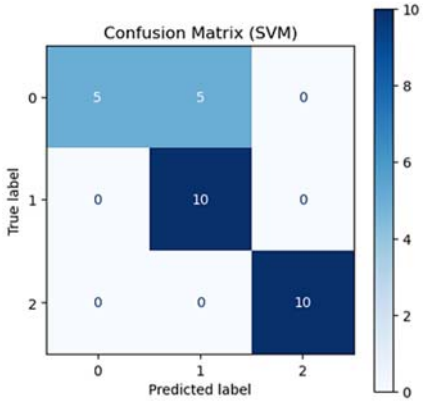

Fig. 17. Confusion matrix of intentional modification.

3.5. Classification Using LiDAR Visualization

Next, classification was performed using the visualized arm position data generated from LiDAR measurements and displayed via the 3D visualizer RVIZ, which is included in the robot operating system (ROS). The arm positions were reconstructed based on the LiDAR point-cloud data and used as inputs for classification. The data used for the analysis were set to 75 cm, corresponding to the LiDAR measurement range shown in Fig. 18. The difference in color is due to differences in reflection.

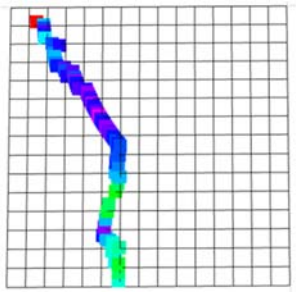

Fig. 18. LiDAR measurement image.

The classification results, confusion matrix, and classification report are presented in Figs. 19 and 20 and Table 2, respectively. In this experiment, Class 0 corresponds to the left-forward position, Class 1 to the right-forward position, and Class 2 to the left-backward position.

Compared with the results obtained using the 8×8 ToF sensor, the classification using LiDAR data showed a greater overlap between the right-forward and left-backward classes. Consequently, the overall classification accuracy decreased to 0.90.

3.6. Classification Results Using Cropped LiDAR Images

The LiDAR measurement data were cropped to a region of approximately 34 cm×34 cm, matching the

measurement area of the 8×8 ToF sensor, and used for classification analysis. The figure from Rivz used here was replotted with the size of each point enlarged such that it looked the same as the 8×8 ToF heatmap, as shown in Fig. 21.

The classification outcomes for both the training and test datasets and the confusion matrix are shown in Figs. 22 and 23, respectively. Although the training data achieved a classification accuracy of 0.90 %, the test data revealed that half of the samples in Class 0 (left-forward position) were misclassified.

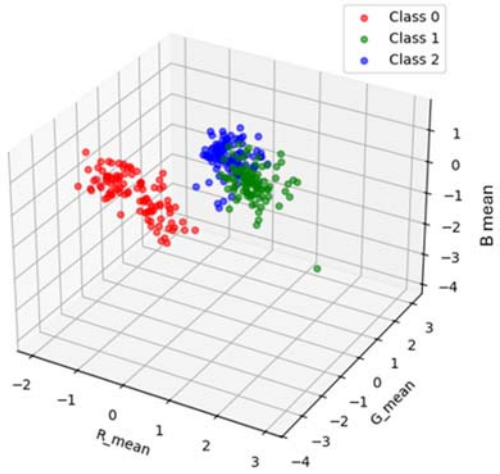

(a) Training data;

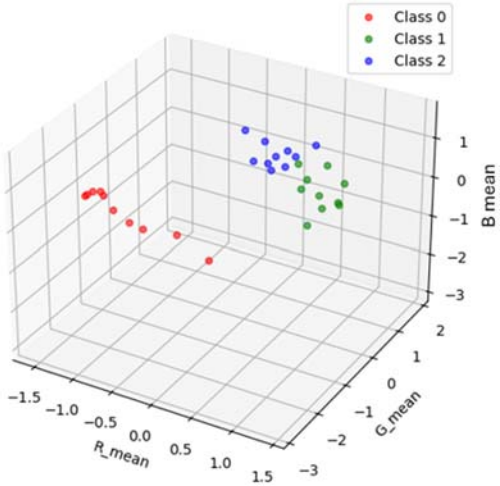

(b) Test data.

Fig. 19. Classification results.

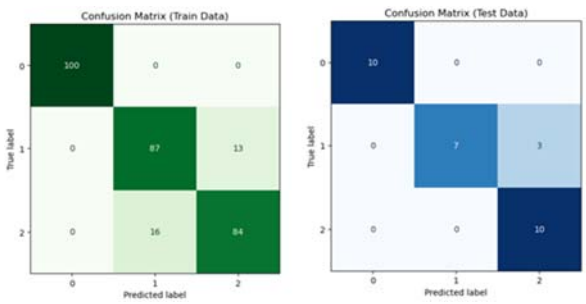

(a) Training data (b) Test data

Fig. 20. Confusion matrix.

Table 2. Precision results.

	precision	recall	f1-score	support
Class 0	1.0000	1.0000	1.0000	10
Class 1	1.0000	0.7000	0.8235	10
Class 2	0.7692	1.0000	0.8696	10
accuracy			0.9000	30
macro avg	0.9231	0.9000	0.8977	30
weighted avg	0.9321	0.9000	0.8977	30

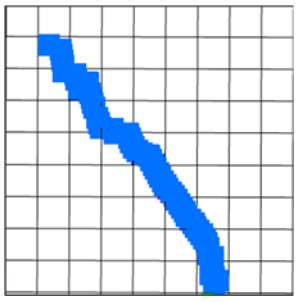

Fig. 21. Cropped LiDAR image.

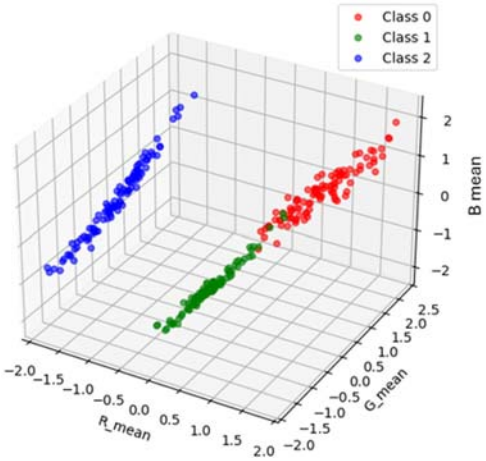

(a) Training data;

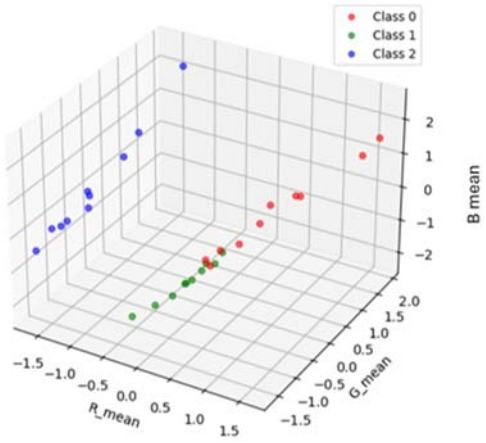

(b) Test data.

Fig. 22. 3D classification plot using cropped LiDAR image.

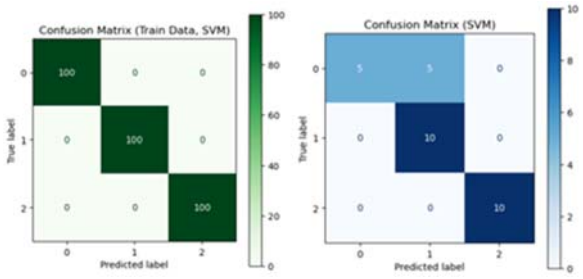

(a) Training data; (b) Test data.

Fig. 23. Confusion matrix using cropped LiDAR image.

3.7. Classification using TensorFlow

Classification was performed using TensorFlow with heatmap images obtained from an 8×8 ToF sensor. The input image resolution varied across four levels: 100×100, 64×64, 8×8, and 4×4 pixels. The initial training was conducted for 10 epochs.

For resolutions up to 8×8, the model loss decreased to nearly zero within 10 epochs, indicating successful convergence, as shown in Fig. 24. However, at the lowest resolution of 4×4 pixels, the model loss remained at approximately 0.6, suggesting reduced classification performance owing to insufficient spatial information.

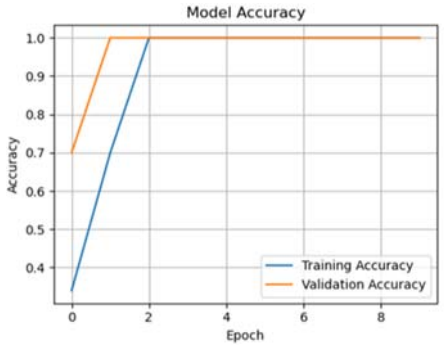

(a) 8×8 pixels;

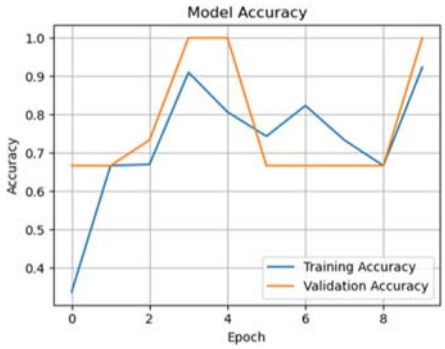

(b) 4×4 pixels.

Fig. 24. Pixel dependence of model accuracy.

To further investigate learning behavior, the number of training epochs was increased to 100. The results are shown in Fig. 25. The model accuracy peaked at approximately 20 epochs, whereas the model loss approached zero after approximately 30 epochs. These findings demonstrate that resolution significantly affects classification performance, and that sufficient training iterations can improve model convergence, even with lower-resolution inputs.

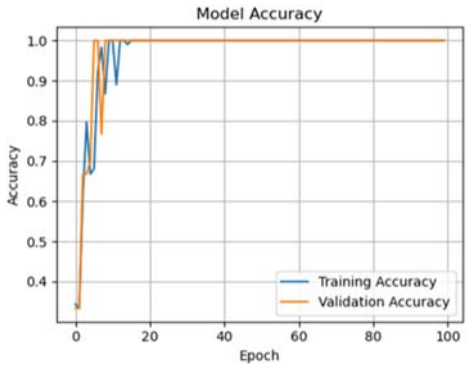

Fig. 25. Model accuracy dependence of epochs.

4. Discussions

4.1. Comparison of Position Accuracy Between 8×8 ToF System and LiDAR System

When the arm was extended forward, the fingertip was positioned approximately 2 cm from the boundary. The forward–backward error decreased as the arm was closer to the participant, which was attributed to the participant's perspective influencing the perceived boundary. In the left–right direction, positional errors were minimal because the lateral location was easier to determine from the perspective of the participant.

In the LiDAR measurement results shown in Fig. 9, the upward and downward movements of the arm were recognized as 2D measurement points observed from the LiDAR located at the origin, resulting in several points plotted in a semicircle. Furthermore, the 8×8 ToF system provides multiple points corresponding to the back of the hand, enabling a more precise estimation of the hand position.

4.2. Classification Using SVM

An investigation into the impact of the LiDAR measurement plot size revealed that, even when the plot size was adjusted to be comparable to that of an 8×8 ToF sensor, the classification accuracy remained at approximately 0.90. This suggests that increasing the plot resolution does not necessarily improve the pattern classification performance.

In this study, the selected regions (top left, top right, and left near the hand) exhibited distinguishable patterns; therefore, differences in plot size did not significantly affect the classification accuracy. However, for more finely segmented regions, such as

the left-center, center-center, right-center, near-center, and near-right (as shown in Fig. 5), detailed LiDAR plot measurements may prove effective in enhancing the classification performance.

4.3. Classification using TensorFlow

In the TensorFlow classification process, three distinct points, the left tip, right tip, and left base of the hand, were selected during the early stages of the study because of their characteristic patterns. Consequently, even when the image resolution was reduced to match the 8×8 segmentation area of the ToF system, the classification accuracy improved within only a few training epochs. This finding suggests that the distinctiveness of these regions facilitates rapid learning.

In contrast, when using 4×4 segmentation, the plot area corresponding to the left base of the hand was significantly narrower, requiring approximately 20 epochs to achieve comparable accuracy. Based on these observations, it can be inferred that increasing the number of training epochs is effective for classifying segmented data into 8×8 regions, particularly when the spatial resolution is preserved.

4.4. Clinical Feedback from Practicing Therapists

Occupational and physical therapists' feedback highlighted the system's clinical relevance and practical potential. Its privacy-preserving quantitative analysis – particularly the numerical evaluation of tabletop activities – was considered noteworthy. Expanding the approach to three-dimensional analysis could broaden the range of assessable motions. However, clearer data presentation is needed to match therapists' data literacy.

5. Conclusions

This study investigated the applicability of two types of ToF-based sensors, an 8×8 ToF sensor and a LiDAR, for upper limb rehabilitation. Although the 8×8 ToF sensor had a limited observation area, it could accurately capture height-related information. In contrast, LiDAR provides a larger volume of data; however, the effective extraction of relevant information requires appropriate filtering. These devices can be selectively utilized depending on the application, and have the potential to contribute to more efficient and quantitative assessments in rehabilitation environments.

The measurement data obtained from the 8×8 ToF system and LiDAR were classified using two methods: SVM and TensorFlow. The SVM approach demonstrated high classification accuracy using RGB image data as features. For LiDAR, the classification accuracy remained nearly equivalent, whether using data extracted from a 75 cm area via the 3D visualizer (rviz) or restricting the area to match that of the 8×8 ToF system. These findings suggest that considering which part of the hand the reflected data originate from may be crucial for improving the classification performance.

Future studies will explore the integration of IMU data with ToF/LiDAR measurements to enable a more detailed trajectory analysis and quantitative evaluation of movement quality. In addition, optimizing sensor placement and developing automated data processing algorithms may reduce measurement errors and enhance usability in clinical settings. Further studies involving larger participant groups are necessary to validate the system under realistic rehabilitation conditions and assess its potential for remote monitoring and privacy-conscious applications.

Acknowledgments

We extend our gratitude to Mr. Y. Fujimori at Seirei Yokohama Hospital. This study was partially supported by the JSPS KAKENHI (grant no. JP23K11207).

References

[1]. M.-C. Jung, S.-J. Kim, J.-J. Rhee, D.-H. Lee, Electromyographic activities of the subscapularis, supraspinatus and infraspinatus muscles during passive shoulder and active elbow exercises, *Knee Surgery, Sports Traumatology, Arthroscopy*, Vol. 24, 2016, pp. 2238-2243.

[2]. H. R. Fazeili, S. K. Venkatesh, Q. Peng, A virtual environment for hand motion analysis, *Procedia CIRP*, Vol. 78, 2018, pp. 127-132.

[3]. I. Pastor, H. A. Hayes, S. J. M. Bamberg, A feasibility study of an upper limb rehabilitation system using Kinect and computer games, in *Proceedings of the 34th Annual International Conference of the IEEE Engineering in Medicine and Biology Society (EMBC'12)*, 2012, pp. 1296-1299.

[4]. A. Rabin, E. Maman, O. Dolkart, E. Kazum, et al., Regaining motion among patients with shoulder pathology – are all exercises equal?, *Shoulder & Elbow*, Vol. 15, Issue 1, 2021, pp. 105-112.

[5]. N. D. Bruyn, L. Saene, L. Thijs, A. Van Gils, et al., Functional recovery of the upper limb after stroke: a systematic review of literature, *Frontiers in Neurology*, Vol. 11, 2020, 597666.

[6]. K. Nagamune, et al., A development of wiping rehabilitation system using leap motion for patients with upper limb paralysis, in *Proceedings of the World Automation Congress (WAC'22)*, 2022, pp. 39-44.

[7]. J. A. Cross, J. deVries, M. Mocarski, N. C. Ketchum, et al., Electromyography of the shoulder musculature during passive rehabilitation exercises, *JSES International*, Vol. 4, Issue 4, 2020, pp. 883-888. X. Liu, X. Zhang, B. Zhang, B. Zhou, et al., An IMU-based ground reaction force estimation method and its application in walking balance assessment, *IEEE Transactions on Neural Systems and*

Rehabilitation Engineering, Vol. 32, 2024, pp. 223-232.
[8]. E. Tijs, T. A. Matyas, Bilateral training does not facilitate performance of copying tasks in poststroke hemiplegia, *Neurorehabilitation and Neural Repair*, Vol. 20, 2006, pp. 473-483.
[9]. L. Oujamaa, I. Relave, J. Froger, D. Mottet, et al., Rehabilitation of arm function after stroke: literature review, *Annals of Physical and Rehabilitation Medicine*, Vol. 52, 2009, pp. 269-293.
[10]. C. Brambilla, R. Marani, L. Romeo, M. L. Nicora, et al., Azure kinect performance evaluation for human motion and upper limb biomechanical analysis, *Heliyon*, Vol. 9, 2023, e21606.
[11]. M. A. Murphy, A. Al-Shallawi, K. S. Sunnerhagen, A. Pandyan, Early prediction of upper limb functioning after stroke using clinical bedside assessment: a prospective longitudinal study, *Scientific Reports*, Vol. 12, 2022, 22053.
[12]. G. Papagiannis, A. Trantafyllou, K. G. Yiannopoulou, G. G. Georgoudis, et al., Hand dexterities assessment in stroke patients based on augmented reality and machine learning through a box and block test, *Scientific Reports*, Vol. 14, 2024, 10598.
[13]. Y. Uchida, E. Ohkubo, T. Funayama, A proposal for an evaluation method of table slide exercise using a MEMS sensor, in *Proceedings of the 10th International Conference on Sensors Engineering and Electronic Instrumentation Advances (SEIA'24)*, 2024, pp. 59-62.
[14]. STMicroelectronics, MEMS Motion Sensor Eval Boards STEVAL-MKI109V3, https://www.st.com/en/evaluation-tools/steval-mki109v3.html
[15]. Y. Uchida, E. Ohkubo, T. Funayama, Application of MEMS sensors in evaluating upper limb rehabilitation, *Sensors & Transducers*, Vol. 267, Issue 4, 2024, pp. 1-8.
[16]. Y. Uchida, E. Ohkubo, M. Nishi, T. Funayama, et al., Application of 8×8 time-of-flight and LiDAR sensors for upper limb rehabilitation: heatmap visualization and positional accuracy evaluation, in *Proceedings of the 11th International Conference on Sensors and Electronic Instrumentation Advances (SEIA'25)*, 2025, pp. 49-53.
[17]. STMicroelectronics, SensorTile.box PRO wireless multi-sensor development kit, https://www.st.com/en/evaluation-tools/steval-mkboxpro.html
[18]. C. López-Franco, L. Villavicencio, N. Arana-Daniel, A. Y. Alanis, Image classification using PSO-SVM and an RGB-D sensor, *Mathematical Problems in Engineering*, Vol. 2014, 2014, 695910.
[19]. C. A. Rivera-Romero, J. U. Munoz-Minjares, C. Lastre-Dominguez, M. Lopez-Ramirez, Optimal image characterization for in-bed posture classification by using SVM algorithm, *Big Data and Cognitive Computing*, Vol. 8, 2024, 13.
[20]. A. Gidudu, G. Hulley, T. Marwala, Classification of images using support vector machines, *arXiv preprint*, 2007, arXiv:0709.3967.
[21]. M. Abadi, et al., TensorFlow: large-scale machine learning on heterogeneous systems, *arXiv preprint*, 2016, arXiv:1603.04467.
[22]. T. Simon, H. Joo, I. Matthews, Y. Sheikh, Hand keypoint detection in single images using multiview bootstrapping, in *Proceedings of the IEEE Conference on Computer Vision and Pattern Recognition (CVPR'17)*, 2017, pp. 4645-4653.
[23]. C. Zimmermann, T. Brox, Learning to estimate 3D hand pose from single RGB images, in *Proceedings of the IEEE International Conference on Computer Vision (ICCV'17)*, 2017, pp. 4793-4801.
[24]. A. Krizhevsky, I. Sutskever, G. E. Hinton, ImageNet classification with deep convolutional neural networks, in Advances in Neural Information Processing Systems, Vol. 25, *Curran Associates, Inc*., 2012, pp. 1097-1105.
[25]. STMicroelectronics, VL53L5CX Time-of-Flight 8x8 multizone ranging sensor with wide field of view, https://www.st.com/en/imaging-and-photonics-solutions/vl53l5cx.html
[26]. GitHub, LetsOKdo/sdk_ld06_raspberry_ros repository, https://github.com/LetsOKdo/sdk_ld06_raspberry_ro